RSC Sustainability

ROYAL SOCIETY OF CHEMISTRY

PAPER

View Article Online
View Journal | View Issue

Open Access Article. Published on 23 December 2025. Downloaded on 3/14/2026 11:47:17 AM.
This article is licensed under a Creative Commons Attribution-NonCommercial 3.0 Unported Licence.

Check for updates

Cite this: *RSC Sustainability*, 2026, **4**, 941

Negative-emission waste-to-concrete *via* tandem supercritical water oxidation and hydrothermal mineralization

David H. Kenney,[a] Andrew M. Charlebois,[a] Shuai Wang,[b] Nima Rahbar,[b] Michael T. Timko[a] and Andrew R. Teixeira*[a]

Received 25th September 2025
Accepted 18th December 2025

DOI: 10.1039/d5su00765h

rsc.li/rscsus

Concrete production and municipal solid waste management contribute up to 13% of global CO_2 emissions. Here, we describe Hydrothermal Oxidation and Mineralization (HTOM) as a new process for production of alternative construction material (ACM) with a compressive strength (9.23 ± 0.98 MPa) more than double what is required for non-loadbearing concrete (4.14 MPa) while storing CO_2. HTOM consists of two oxidative reactions: (1) supercritical water oxidation (SCWO) converts the organic fraction of food waste to a high-pressure CO_2 stream while producing thermal bioenergy that can be recovered using a turbine, then (2) the high-pressure CO_2 stream is used for rapid mineralization of soluble calcium to calcium carbonate, reaching 100% conversion within 20 minutes. ASPEN/HYSYS simulations and a GREET lifecycle analysis demonstrate that HTOM has the potential to offset 0.1 kg of CO_2 per kg of ACM produced by simultaneously diverting fugitive landfill emissions, capturing waste energy, and offsetting traditionally CO_2-intensive concrete mortar production.

1. Introduction

Negative emission technologies (NET) are required to ensure a sustainable future for our planet.[1] Collectively, two industries, (1) municipal solid waste (MSW) management and (2) concrete production, are responsible for 8–13% of the 52 billion tons of annual $CO_{2,eq}$ emissions,[2–4] with predicted greenhouse gas emissions from these industries reaching 3.4 and 5 billion tons, respectively, by 2050.[2,3,5,6] The carbon content embodied in the 2 billion tons of MSW produced annually closely matches the carbon released when producing the 4 billion tons of Ordinary Portland Cement that is required to satisfy the global concrete demand, presenting an attractive opportunity to couple these industries with one another. To create a more circular carbon economy, substantial efforts have focused recently on CO_2-to-fuels and CO_2 upcycling to chemicals and other products. However, life cycle assessments have shown these technologies to, at best, be net-zero and, at worst, net carbon-emitting during production and at the end of life.[7,8] An effective solution must (1) incur minimal energy and carbon penalties in the conversion of CO_2 to a valorized product, (2) have an ultimate fate that durably sequesters carbon, and (3) displace or offsets a carbon-intensive product at a globally relevant scale. Our proposed waste-to-concrete process, shown schematically in Fig. 1, can efficiently accomplish all three goals.

Favorable thermodynamics and kinetics are critical to the efficiency of any process. In terms of thermodynamics, the production of Ordinary Portland Cement (OPC), the most common form of cement, relies on the calcination of calcite ($CaCO_3$) to form calcium oxide (Fig. 1a), a highly energetically unfavorable process requiring +1129 kJ mol^{-1} C^{-1}.[9,10] Overcoming this thermodynamic barrier requires calcite, along with clays, to be fired in a kiln (Fig. 1b) at 1200 °C to liberate CO_2, bind calcium oxide (CaO) with silica (SiO_2), and form calcium silicates (*i.e.*, $CaSiO_3$), the eventual source of strength in concrete.[11,12] The calcination step accounts for 90% of the greenhouse gas (GHG) production during OPC production, with 50% resulting from the release of CO_2 from calcite and the remaining 40% from fuel combustion.[11] Efforts to decarbonize the built environment have focused on primarily on OPC production, specifically investigating the use of green fuels and electrified production, novel mineral sources, as well as alternative geopolymers.[13,14] Notably, however, these prior approaches have not been successful in integrating low-footprint carbon sources or achieving the necessary mineralization rates required to sequester carbon feasibly. Beyond cement and concrete, efforts have been dedicated to engineer timber to sequester carbon and support the construction markets, but these materials face concerns of durability and fire resistance.[15] This study evaluates the use of MSW as a negative emission carbon source. According to the EPA, most waste (50%) is landfilled in the United States (Fig. 1b), and more than

[a]*Department of Chemical Engineering, Worcester Polytechnic Institute, Worcester, Massachusetts 01609, USA. E-mail: arteixeira@wpi.edu*

[b]*Department of Civil, Environmental, and Architectural Engineering, Worcester Polytechnic Institute, Worcester, Massachusetts 01609, USA*

© 2026 The Author(s). Published by the Royal Society of Chemistry

Open Access Article. Published on 23 December 2025. Downloaded on 3/14/2026 11:47:17 AM.
This article is licensed under a Creative Commons Attribution-NonCommercial 3.0 Unported Licence.

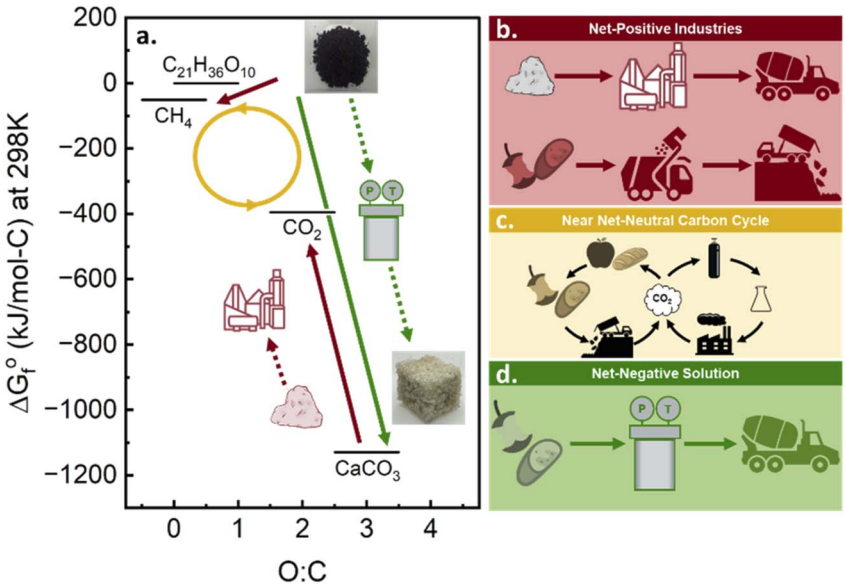

Fig. 1 Schematic of the thermodynamic landscape for current and proposed industrial pathways. (a) Overall thermodynamic path for the linear MSW management and concrete processes (b, red), CO_2 reduction/combustion processes (c, yellow), and by contrast, energy favorable release for oxidative bioenergy carbon capture and utilization (BECCUS) strategies explored here (d, green). The proposed pathway will leverage the favorable oxidative thermodynamics to convert organic carbon in MSW to alternative concrete.

80% is organic.[16] Once a landfill is sealed, the organic wastes undergo anaerobic digestion to form methane (Fig. 1a). Which has a global warming potential (GWP) 28 times that of CO_2.[16–18] For landfilled food waste, this translates to a corresponding GHG emission rate of 1.52 kg CO_2 per kg waste.[19]

Carbon dioxide or equivalent landfill gases are released into the atmosphere and are rapidly diluted, requiring exorbitant energy and capital demands to concentrate it; the currently estimated energy input required for DAC processes is 4.5 MJ kg^{-1}, with costs ranging from 125 to 335 \$ per ton.[20,21] An alternative option for carbon removal from the atmosphere is by mineralization, which is an aqueous chemistry that produces an insoluble mineral product that is not affected by the presence of oxygen.[22–24] Again, with a diluted feed like atmospheric CO_2, the process is energy intensive and requires a large footprint to concentrate enough CO_2 to improve kinetic rates. Carbon utilization of recovered carbon has typically focused on reductive processes, which are thermodynamically unfavorable (Fig. 1a);[25] Moreover, many of the reduced products are intended for combustion as fuels, thereby releasing CO_2 back into the atmosphere in a wasteful well-to-wheel life cycle (Fig. 1a). The need for more energy-efficient, cost-effective, durable, and scalable options is urgent.

Here, we demonstrate a new technology, which is kindred to bioenergy and carbon capture, utilization, and storage (BECCUS),[26] and that leverages the carbon and energy in wet organic MSW to develop the next generation of alternative construction materials (ACM). The new process, termed hydrothermal oxidation and mineralization (HTOM), couples supercritical water oxidation (SCWO) and high-pressure mineralization to rapidly convert wet organic waste feeds into pressurized CO_2 that readily converts soluble calcium into structured $CaCO_3$. While SCWO has been studied since the 1980s as an effective hazardous waste treatment method,[27] the extreme corrosive environment, high pressures and moderately high temperatures have created an environment that has traditionally been challenging to scale safely and effectively.[28,29] The current study recognizes this, and lays out a strategy for distributed application of SCWO while also recognizing that innovation in technological implementations of SCWO remain necessary. Here, we find a novel use for SCWO as an efficient means of converting wet organic waste into a high-pressure CO_2 stream and performing mineralization in the presence of renewable polymers such as gelatin to confer strength to the ACM. Due to its thermodynamic favorability, HTOM has the potential to be net energy generating; and by producing a form of carbon that can be durably stored and used in large-scale applications, the entire process can be a negative emissions technology (NET). Therefore, the goal of this work is to confirm the thermodynamic efficiency of the new process, evaluate rates of key steps to assess technological efficiency, and use this data to perform material and energy balances to quantify its CO_2 abatement potential.

2. Results

2.1. SCWO of food waste to produce high-pressure CO_2

Representative food waste was obtained from the New Hampshire VA Hospital (Manchester, NH) and used for SCWO experiments. Details about the food waste composition can be found in SI Table S1. The SCWO of food waste was conducted using hydrogen peroxide as the model oxidant molar with loadings ranging from O : C = 0–3 (SI Table S2). Reactions were run at 400–450 °C for 1 hour, allowing the system to reach autogenous pressures of 211–265 atm (Fig. 2a). When the reaction was run in the absence of oxidant (O : C = 0), the

 © 2026 The Author(s). Published by the Royal Society of Chemistry

Open Access Article. Published on 23 December 2025. Downloaded on 3/14/2026 11:47:17 AM.
This article is licensed under a Creative Commons Attribution-NonCommercial 3.0 Unported Licence.

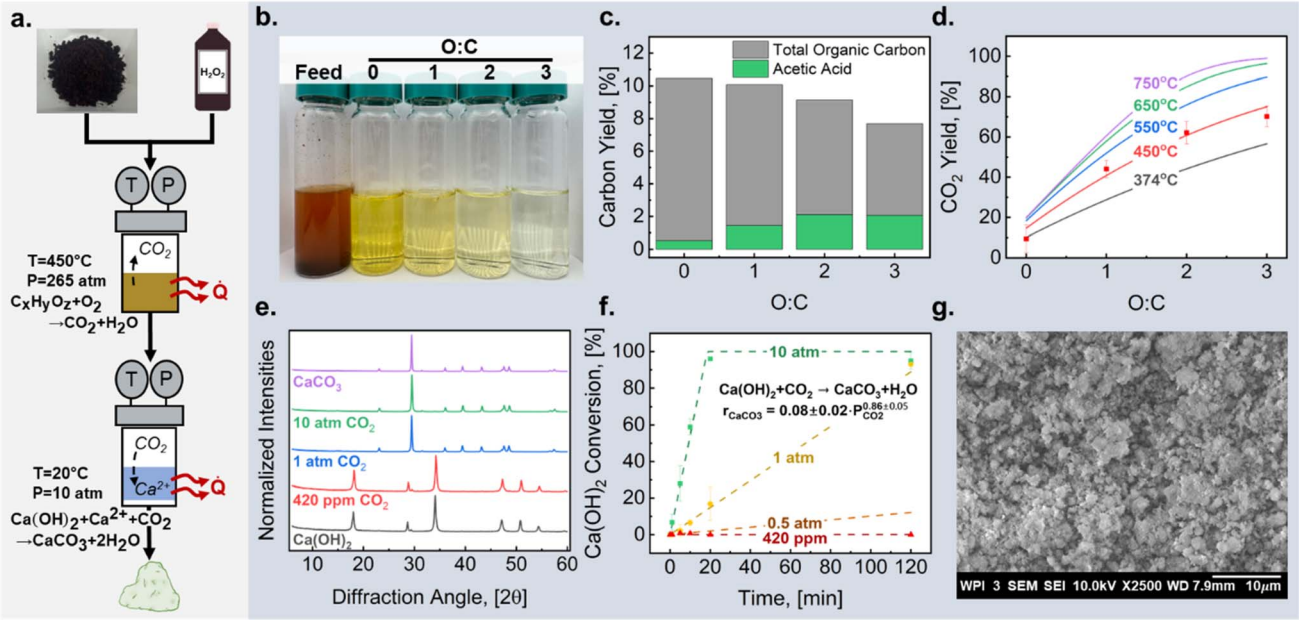

Fig. 2 Analysis of the hydrothermal mineralization pathways. (a) Schematic of the two-stage SCWO-Mineralization process for waste-to-concrete. (b–d) SCWO oxidation showing recovery of organics from aqueous phase with developed model for predicting gas-phase CO_2 yields: $r_{CO_2} = 10^{-1.13}\exp\left(\frac{-25.3}{RT}\right)[FW][O_2]^{0.65}$. (e–g) Hydrothermal mineralization showing complete conversion to calcite achievable within 20 min at CO_2 pressures corresponding to SCWO product streams. All error bars represent the standard deviation within a given sample set (N = 2).

primary product was an organic-rich liquified product.[30,31] The gas product was primarily CO_2 which accounted for less than 10% of the total carbon product (SI Fig. S1). In comparison, reactions with O : C > 0 (*i.e.*, SCWO conditions) produced primarily gases and water-soluble side products (SI Fig. S1). The gas product consisted primarily of CO_2, with yields of 40–70% at 450 °C (SI Fig. S1); elevated temperatures have been demonstrated to achieve quantitative conversion on the order of seconds,[32] consistent with our model predictions at 650 °C (Fig. 2d). For all reaction conditions, aqueous products were also collected, consisting of a mixture of small chain carboxylic acids (SI Fig. S2) and aromatic compounds (SI Fig. S3). Increasing the initial oxidant loading from O : C = 0 to O : C = 3 shifts the products from solid and liquefied products to gases, which is evident both by product analysis accompanied by a noticeable change in the aqueous phase color, from yellow (at O : C = 0) to colorless (at O : C = 3) and as shown in Fig. 2b. The change in aqueous phase color corresponds to a reduction in aromatic compounds corresponding to a decrease in UV-Vis absorbance at 220 nm (SI Fig. S3). The concomitant reduction of aqueous carbon and simultaneous increase in small chain carboxylic acids (Fig. 2c) and gaseous CO_2 yield (Fig. 2d) observed with increasing initial O : C ratio is consistent with greater completion of the desired oxidation reaction, converting food waste to CO_2.

To maximize the usefulness of the experimentally determined conversion data, Fig. 2d contains a simple theoretical prediction of yield at temperatures above 450 °C. The model is based on previously published studies and consists of lumped reactions that are assumed to be first order relative to food waste.[33] The regressed value of the apparent activation energy is 25.3 kJ mol^{-1}, is comparable to previously published values for food waste combustion.[33,34] More information on the fitting methodology can be found in the SI. The predictions show that full conversion can be achieved at temperatures near 650 °C, again consistent with previous studies of SCWO that have published complete conversion of aqueous-soluble compounds from 500–600 °C.[35–38] The kinetic model therefore validates that the experimental data are consistent with previous SCWO studies and provides confidence in using the data in subsequent analyses. Experimental data were used in all subsequent analyses.

2.2. Rapid and complete mineralization of high-pressure CO_2

Supercritical water oxidation of food waste at 450 °C produces an autogenous headspace pressure of 265 atm (Fig. 2a). Industrial flue gas point source capture (PSC) and atmospheric direct air capture (DAC), by contrast, are available at ambient pressure; the thermodynamic benefit of pressurization is quantified by the minimum work of separation, which depends on the fugacity – and hence the partial pressure – of the separated gas. The minimum work of separation for capturing CO_2 from DAC or natural gas or coal combustion PSC is found to range from 7–25 kJ mol^{-1} of CO_2.[39] For O : C = 3 the headspace results in a 35 vol% CO_2 stream which would reduce the work of separation to 4 kJ mol^{-1} of CO_2 at ambient conditions.[40]

A pressurized CO_2 stream can achieve extreme aqueous supersaturation that accelerates mineralization rates, potentially solving the footprint problem that plagues industrial gas capture and DAC.[41,42] To quantify the impact of CO_2 partial

Open Access Article. Published on 23 December 2025. Downloaded on 3/14/2026 11:47:17 AM.
This article is licensed under a Creative Commons Attribution-NonCommercial 3.0 Unported Licence.

pressure on mineralization kinetics, rates were measured at three partial pressures for the conversion of calcium hydroxide ($Ca(OH)_2$) to calcium carbonate ($CaCO_3$): (1) 10 atm CO_2 (simulating HTOM conditions), (2) 1 atm CO_2 (PSC), and (3) 420 ppm CO_2 (DAC). The pressure of the HTOM stream was selected as a conservative lower limit that accounts for partial depressurization associated with cooling the SCWO product gas and dilution due to the presence of N_2 when air is chosen as the oxidant source. The pressure of the PSC stream, on the other hand, is an upper limit on the partial pressure of CO_2 in a combustion gas mixture, with most flue gasses ranging from 4–14 wt%.[43] Using $Ca(OH)_2$ as the precursor ensures that the slurry pH will be sufficiently alkali to ensure that CO_2 will form carbonic acid to react with $Ca(OH)_2$ to form $CaCO_3$ (SI Fig. S4).

Exposing water slurries of $Ca(OH)_2$ to CO_2 streams at room temperature for 2 h resulted in the formation of solid products, which were then analyzed using XRD to distinguish and quantify formed $CaCO_3$ from residual $Ca(OH)_2$ (Fig. 2e). Subsequent kinetic mineralization studies were performed (Fig. 2f), showing that $Ca(OH)_2$ conversion to $CaCO_3$ was complete after 20 min exposure to the HTOM stream. In contrast, the process reached completion only after 2 h for the ideal PSC stream. Negligible conversion was observed for the $Ca(OH)_2$ exposed to the CO_2 stream simulating DAC conditions. Theoretical modeling was performed to estimate the mineralization rate of a less optimistic PSC than shown in the experimental data provided in Fig. 2f, showing that a PSC stream consisting of 10% CO_2 at 1 atm (*i.e.*, partial pressure of 0.1 atm) increases the rate marginally compared with the DAC stream (4.2×10^{-4} atm). Accordingly, Fig. 2f confirms that the pressurized product stream accelerates mineralization at least 10-fold relative to that observed for combustion gas streams and more than 100-fold relative to DAC. These rate increases correspond directly to commensurate decreases in the footprint required for mineralization.

The $CaCO_3$ product formed from exposure of $Ca(OH)_2$ to the HTOM gas stream consisting of 10 atm CO_2 was imaged using FESEM (Fig. 2g). The mineralized product is a uniform distribution of nearly spherical calcite particles ranging in size from 1–3 μm (Fig. 2g). Due to the rapid mineralization kinetics observed in this system, the rate of nucleation is must be much larger than the rate of growth of calcite particles, resulting in small particle sizes and a narrow size distribution.[44] A small, uniform crystal size is crucial to developing alternative concretes as this allows for the use of finer aggregate grain sizes, increasing the potential for compressive strength in mineralized concrete mortars.[45,46]

2.3. HTOM for production of ACM

Having proven thermodynamically favorable, rapid, and complete conversion of $Ca(OH)_2$ into $CaCO_3$, the next step was to combine the mineralization step with ACM synthesis. Reported cementation efforts using mineralization chemistries use enzymes or microbes to increase the effective concentration of carbonic acid in the aqueous phase.[41,47] HTOM allows for rapid gas–liquid mass transfer and subsequent calcite precipitation without the assistance of biological promoters, thereby reducing costs and process complexity. To study the use of HTOM for ACM production, mineralization was performed in the presence of sand and gelatin to confer strength.[41] Three combinations of mortar were tested (shown schematically in Fig. 3a): (I) sand + gelatin + $Ca(OH)_2$ (Fig. 3 red), (II) sand + gelatin + $CaCl_2 \cdot 2H_2O$ + Tris base (Fig. 3, green), and (III) sand + gelatin (Fig. 3, black). $Ca(OH)_2$ provides a stoichiometric amount of hydroxide ions (OH^-) to neutralize carbonic acid, which otherwise prevents the dissolution of CO_2 molecules at lower pH values (SI Fig. S7) and also Ca^{2+} ions to form the calcite; unfortunately, the resulting material formed in the experiment (I) is weak (Fig. 3b, red circle). The SEM images of this material show calcite to be grain-coating, but no bridging occurs between individual sand grains (Fig. 3a). Grain–grain bridging is thought to be required for ACM strength[41] Experiment (II), which uses $CaCl_2 \cdot 2H_2O$ as a water-soluble calcium precursor and Tris base to maintain alkali pH, results in an ACM exhibiting bridging between sand grains as well

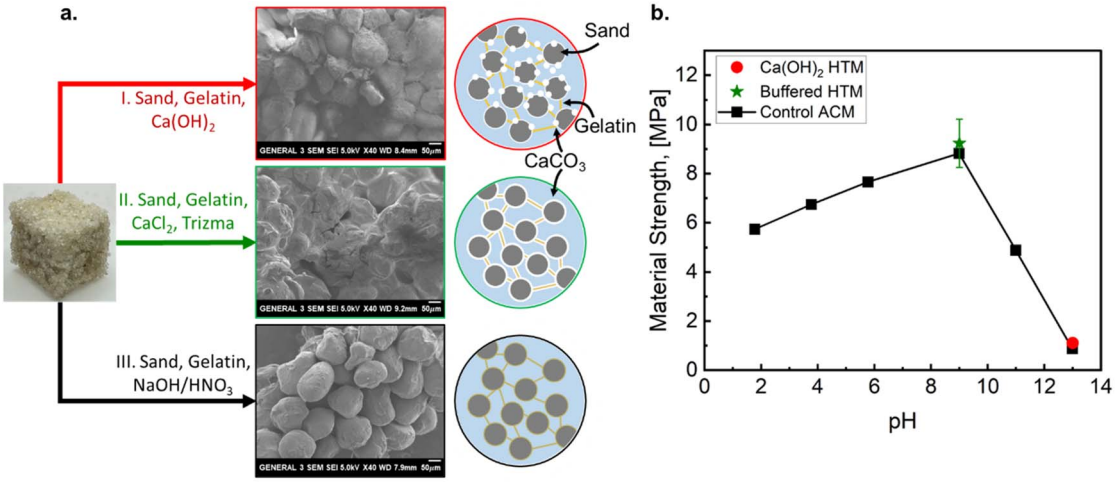

Fig. 3 Overview of the integration of hydrothermal mineralization with alternative concrete mortars. (a) green concrete castings are formed after exposing the wet sand, gelatin blends for (red) unbuffered $Ca(OH)_2$, (green) buffered $CaCl_2$, and (black) calcium-free controls to 10 atm CO_2 at 25 °C for two hours. (b) strength is imparted by the scaffolded gelatin structure, with the pH-controlled calcite-infused ACM exhibiting optimal strength at pH = 9. All error bars represent the standard deviation within a given sample set ($N = 4$).

 © 2026 The Author(s). Published by the Royal Society of Chemistry

Open Access Article. Published on 23 December 2025. Downloaded on 3/14/2026 11:47:17 AM.
This article is licensed under a Creative Commons Attribution-NonCommercial 3.0 Unported Licence.

as a nearly 1000% increase in compressive strength relative to experiment (I) and without the need for biological promoters (Fig. 3b, green star).[41] The compressive strength of the resulting ACM was 9.23 MPa, more than double that required for non-load-bearing concrete (4.14 MPa) and nearly sufficient for load-bearing masonry units (13.8 MPa).[48,49] Fig. 3b shows that $CaCl_2$ and Tris base buffer produce an ACM with sand particles covered with calcite and abundant grain–grain bridging. The produced ACM material has a density of 1.45 ± 0.04 g ml^{-1}, 66% of the density of OPC (2.2 g ml^{-1}).[41] When the strength is normalized to the density, the ACM has equivalent specific strength (6.37 MPa ml g^{-1}) compared with load-bearing concrete (6.27 MPa ml g^{-1}).

Experiment (III) was performed over a range of pH values but in the absence of calcium. Interestingly, the strength of materials produced in experiment (III) is highly dependent on pH and – at optimal pH – results in a material with strength comparable to that observed for experiment (II) (sand + gelatin + $CaCl_2 \cdot 2H_2O$ + Tris base). Experiment (III) confirms that controlling pH is required for production of an ACM with favorable properties.

The strength of the material synthesized in the absence of calcium indicates that gelatin–sand interaction is the key, with the disposition of calcite playing a negligible role. Gelatinization is optimized at a pH of 9, coincident with the pH of the buffered mixture used in the experiment (II) (Fig. 3b, green star). At a pH differing from 9, either in the alkali or acidic direction, the gelatin triple helices cannot crosslink during dehydration, leading to materials with less strength than those produced by crosslinking at optimal pH (Fig. 3b).[41,50] In comparison, experiment (I) was performed at a pH much more alkali than the optimal value. Imaging the material produced from the experiment (I) reveals well-defined yet highly agglomerated individual particles; agglomeration associated with the gelatin, rather than bridging, confers material strength. Accordingly, ACM formed by calcium mineralization depends on gelatinization while durably storing CO_2 as $CaCO_3$.

2.4. Carbon negativity

Having established technical feasibility, the next step was to evaluate the carbon balance for HTOM using experimental data reported here. Mass and energy balances were solved using ASPEN/HYSIS and combined with life cycle analysis tools to estimate the CO_2 produced – or abated – by the production of ACM (Fig. 4). More details are provided in SI Fig. S5 and Table S3. Fig. 4a shows the overall energy balance for converting food waste to $CaCO_3$ as a function of initial solids and oxidant loadings. Hydrothermal liquefaction (*i.e.*, O : C = 0) is an endothermic process, with substantial energy required to maintain the primary reactor vessel at 450 °C. For SCWO reactions (O : C = 1–3), the oxidation and mineralization steps recover nearly 50% of the initial energy in the feed. The energy balance is relatively insensitive to O : C ratio if it is greater than 2 and only weakly dependent on solids loading, indicating that economically realistic O : C ratios can achieve favorable energy returns for feeds with solids loadings that can be pressurized using existing high-pressure pumps. A detailed breakdown of the energy balance can be found in SI Fig. S6.

The mass and energy balances from Fig. 4 were combined with data from GREET, a lifecycle database developed by Argonne National Laboratory with predefined hydrothermal processes, for a process-level LCA. The LCA was performed using experimental data obtained at 450 °C and an O : C ratio of 3. The ACM material in this LCA is considered a drop-in replacement for concrete as it currently has strength that outperforms non-load-bearing concrete (4.14 MPa).

Fig. 4b compares the sequential effects of several process variations between traditional concrete and food waste management against the production of ACM with varying carbon contents. The net emissions between the two industries are representative of the total offset potential of ACM production in avoiding the production of concrete and diversion of food waste from traditional waste management. Traditional concrete production results in 0.1 kg CO_2 per kg concrete (light gray, Fig. 4b). In comparison, ACM production without including sequestered carbon produces 0.02 kg CO_2 per kg ACM corresponding to a net reduction of −0.076 kg CO_2 per kg concrete. Carbon offsets included aversion of CO_2 and CH_4 arising from food waste landfilling when carbon is sequestered within the ACM. The magnitude of this offset depends on the

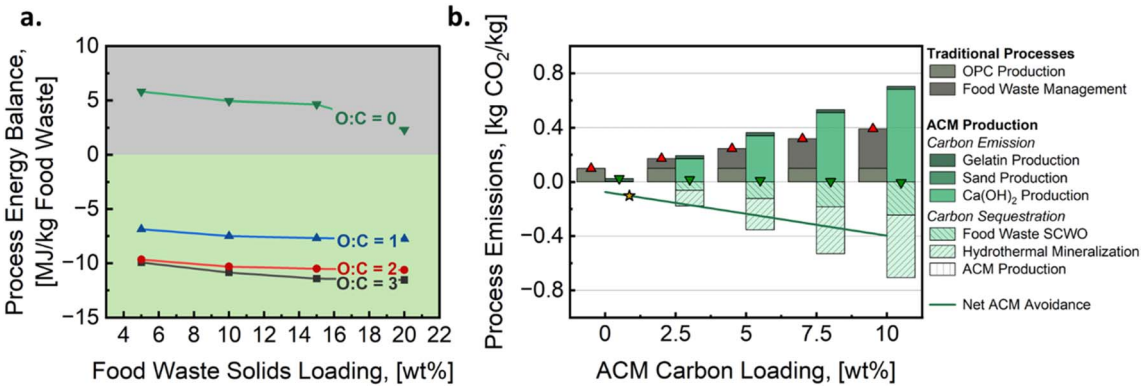

Fig. 4 (a) Process modeling for the combined SCWO + mineralization steps demonstrates the potential for autothermal operation (0 MJ kg^{-1}) or even as a net energy-producing process as oxidant and solids loading is increased. (b) Life cycle assessment shows positive and negative emission processes (solid and shaded bars, respectively) of the combined HTOM process demonstrates that the overall process can displace 0.1 kg CO_2 per kg alternative concrete for conditions in this study (yellow star).

Open Access Article. Published on 23 December 2025. Downloaded on 3/14/2026 11:47:17 AM.
This article is licensed under a Creative Commons Attribution-NonCommercial 3.0 Unported Licence.

amount of carbon contained in the ACM. Experimentally, the target carbon loading was 0.72 wt%;[41] the measured ACM material produced by HTOM contained 0.40 wt% of carbon. More details are provided in SI Fig. S7 in the SI. With this carbon content in the ACM, CO_2 removal for the HTOM process is −0.1 kg CO_2 per kg ACM, which is effectively 0.1 kg of CO_2 averted for every kg of ACM that is produced.

3. Discussion

HTOM achieves (1) conversion of organic wastes into a high-pressure CO_2 stream, (2) rapid and complete mineralization of CO_2 as carbonate, (3) production of an ACM with a compressive strength of 9.23 MPa, and (4) net carbon negativity relative to standard waste management and concrete production. The scale of global organic waste generation is on the same order of magnitude as concrete demand, meaning that the magnitudes of the supply and demand streams are well matched as required for a scalable technology.[5,6] Despite the abundance of energy-rich organic wastes, these feeds are currently disposed of in landfills, incinerators, or digestors. The use of these organic wastes for ACM production has the potential to offset nearly a fifth of all anthropogenic greenhouse gas emissions.[9–11] Strategic use of these wastes could be one key to unlocking a climate technology that aids in the reduction of anthropogenic carbon at a scale with real potential global impact.

Any technology that aims to utilize wastes for carbon storage must: (1) achieve a thermodynamic pathway that favorably concentrates then sequesters CO_2, (2) be atomically and kinetically efficient to carbon in each stage of the sequestration process, (3) create a valorized product that is a drop-in replacement for existing building materials, and (4) exhibit a net-negative carbon demand, including the sourcing of all system inputs at scale. The current study establishes that HTOM achieves all of these goals.

First, from a thermodynamic perspective, this study identifies a pathway to concentrate high-pressure/temperature CO_2 without incurring the separation and regeneration penalties of DAC. The demonstrated process hydrothermally oxidizes the energy-rich, wet organics, releasing 8.4 MJ kg^{-1} of food waste and producing a stream of high-pressure CO_2. Energetics benefit because SCWO is strongly thermodynamically downhill and does not require energy-intensive drying; pressurization of the feed itself is a low-energy process due to its liquid state. The high-pressure CO_2 is then mineralized to form calcium carbonate within a concrete matrix. This step is thermodynamically downhill ($\Delta G = -1129$ kJ mol^{-1}) and releases an additional 3.2 MJ kg^{-1} FW of bioenergy. Compared to current direct and point source capture technologies, HTOM is thermodynamically favorable, highly selective to CO_2, and robust enough not to be affected by residual oxygen or moisture as the reaction is facilitated in water.

Second, the study demonstrates the rapid supercritical water oxidation of a real wet MSW feed. Specifically, food waste was chosen for this study as it is energy-rich, cost-negative and exists at a scale that closely matches the demand by the ACM process.[31,51] Experimental results indicate that food waste can be converted with a 70% yield of CO_2 at 450 °C; theoretical models suggest that operating at 650 °C can achieve 100% yield on the order of minutes, which can provide further benefits.[32] Due to the extreme supersaturation imposed by the HTOM-produced CO_2, the mineralization step reaches completion in just 20 min, at least 10-fold faster than is possible for PSC and more than 100-fold faster than DAC.

Third, HTOM produces an alternative concrete matrix with 9.23 MPa strength, making it a competitive alternative for non-load-bearing concrete, and very close to the average strength required for load-bearing masonry units (13.8 MPa), a product responsible for 6% of the global concrete production.[49,52] The current design uses gelatin polymers to confer strength *via* crosslinking upon dehydration. However, a pH more acidic or alkaline than the optimal value (9) prevents crosslinking and reduces the strength. In the current, buffered synthesis, SEM-EDS imaging confirms that residual Cl counterion remains in the final ACM product that is sourced from $CaCl_2$ (SI Fig. S8). While the direct impact on long-term durability due to the Cl is unknown, future development of a chloride- and buffer-free synthesis should consider polymer matrices that are stable at elevated pH, allowing for the direct use of $Ca(OH)_2$ without the use of a buffering salt. A strengthening agent that is stable in alkali environments would enable a process that can retain strength without the pH control requirement. Furthermore, by more carefully controlling the nucleation and growth kinetics during mineralization, the materials may be engineered to both increase the carbon loading (up to 12 wt% C is theoretically possible) or strength—native limestone ranges from 10–50 MPa, which is comparable to OPC (56 MPa).[53,54] While the long-term stability of the ACM was not studied in this work, it is important to acknowledge that the reversible hydrolysis of the biopolymer binder should be carefully considered in future developments of such technologies, as other composite materials have experienced similar challenges.[55–57] Though gelatin was combined with a buffer and used effectively as a biobinder here, future development of polymeric binders that can be produced sustainably at the scale of 1–4 billion ton per year and are stable under highly caustic and aqueous environments are required to further advance this field.

Fourth and finally, life cycle analysis of the HTOM process establishes its potential as a negative emissions technology by yielding a net reduction of −0.1 kg CO_2 per kg ACM. Accordingly, the process presents a significant opportunity for energy generation, waste disposal, concrete production, and carbon storage. While the studied process was not optimized for a complete technoeconomic analysis (TEA), existing literature for SCWO and hydrothermal liquefaction (HTL), an adjacent hydrothermal technology, supports the development of HTOM as a cost-competitive solution as it is a localized solution that valorizes products on the front and back-end of the process.[58,59]

In the future, further improvements are possible. Evaluating the GHG breakdown (Fig. 4b) shows that the primary emissions contribution to ACM production is the use of calcium hydroxide. This study assumes that calcium hydroxide is produced through the chloroalkyl process from calcium brines that have been concentrated to the solubility point of calcium

 © 2026 The Author(s). Published by the Royal Society of Chemistry

Open Access Article. Published on 23 December 2025. Downloaded on 3/14/2026 11:47:17 AM.
This article is licensed under a Creative Commons Attribution-NonCommercial 3.0 Unported Licence.

chloride (74.5 g per 100 ml). While this step is energy intensive and has a carbon footprint of 1.09 kg CO_2 per kg $Ca(OH)_2$, this alternative production of $Ca(OH)_2$ nets a 13% decrease in emissions from the traditional production (1.26 kg CO_2 per kg $Ca(OH)_2$), which usually relies on hydrating lime (CaO) produced through the calcination of $CaCO_3$. Future innovations toward the electrification of the $Ca(OH)_2$ process could help reduce the emissions associated with $Ca(OH)_2$ production by an additional 50%, a crucial step in deploying green concrete mineralization technologies such as HTOM. Electrified and alternative synthesis routes that source the calcium hydroxide from $CaCl_2$ followed by electrochemical oxidation, mined minerals such as wollastonite or waste cement may be more attractive calcium sources with smaller carbon footprints.[60–62]

In conclusion, the present study presents a compelling case for HTOM as a negative emissions technology that can avert up to 13% of global GHG emissions. To secure a more sustainable future for our planet, continued work on ACM and other NETs must focus on process scaleup and technoeconomic considerations, particularly with regard to the rapid setting of the ACM blocks at mild temperatures and pressures.

4. Methods and materials

4.1. Supercritical water oxidation of food waste

Greener Chemistry LLC provided the food waste in this study. The waste was collected from a veteran's hospital, dehydrated and ground using an Ecovim dehydrator, and then stored in a freezer at −20 °C until used. All SCWO occurred in a Parr Series 4756A batch reactor (SI Fig. S9 and S10) constructed of 316 SS with an internal volume of 250 ml. Each run reacted 1 g of dehydrated food waste in 50 ml of deionized water. The oxidant source for the reaction was 30 wt% hydrogen peroxide that was loaded into the reactor at various amounts to achieve different oxygen-to-carbon (O : C) ratios of 0–3 on a molar basis. Molar ratios were not corrected for oxygen present in the food waste. All reactions were run at or below 450 °C and produced autogenous pressures of 204–265 atm (SI Table S1). Reactions beyond 450 °C and O : C = 3 were not evaluated for the risk of reactor failure. The reactor was rated for 500 °C and 340 atm and was fitted with a rupture disk to allow for a controlled failure route in an emergency. Additionally, since the primary oxidant source in these reactions was hydrogen peroxide, care was taken to inspect the reactor walls for pitting as high concentrations of H_2O_2 at high temperatures have been shown to corrode stainless steel.[63]

4.2. Product analysis and yields

Upon the completion of the reaction at 60 min, the reactor was cooled in a cold-water bath to 40 °C in <10 min. The headspace was vented into a volumetric collection vessel to measure the total headspace volume by water displacement (SI Fig. S9). The collected gas was then sampled with a gas-tight syringe. It was injected onto a Shimadzu GC-2014 at 80 °C with a RESTEK Rt®-Q-BOND column, 25 ml min^{-1} helium carrier gas, and TCD at 110 °C inlet to determine the volume fraction of CO_2 which was determined using a calibration of known CO_2 injection volumes. Peaks for nitrogen and carbon dioxide were individually calibrated using volumetric injections of standard gases (SI Fig. S11). Carbon recovery for this study is defined as the mass of carbon recovered in the gas head space as CO_2 ratioed against the mass of carbon in the initial feed. After analyzing the gas headspace, the reactor contents were separated *via* vacuum filtration to separate the aqueous product from char using methods described in prior work by the group. In hydrothermal liquefaction, an oil phase is known to attach itself to the char phase, so the char was washed with acetone to separate any oil that may have formed but was not quantifiable except in the oxidant-free control (O : C = 0). The aqueous product was analyzed on a Shimadzu TOC-L system to determine the total organic carbon within the aqueous phase. Aqueous acetic acid concentrations were analyzed on a Shimadzu HPLC equipped with a RESTEK ROA-Organic Acid H + (8%) column at 50 °C with a flowrate of 0.6 mL min^{-1} (SI Fig. S3).

4.3. Modeling the SCWO mechanism

The reaction pathway for this study was modeled as the direct oxidation of food waste to CO_2 and all remaining carbon in the system was considered to remain as food waste.

$$r_{CO_2} = A_{CO_2}\exp\left(-\frac{Ea_{FW}}{RT}\right)[FW]^n[O_2]^m \quad (1)$$

where r is the rate of consumption of food waste in the reactor, A_{CO_2} is the model pre-exponential factor, Ea_{FW} is the apparent activation energy for the system R is the ideal gas constant, T is the temperature, [FW] and $[O_2]$ are the concentrations of food waste and oxygen in the system, all with units of J, mol, L, K, and sec. The concentration of food waste was determined using an estimated molecular formula ($C_{21}H_{36}O_{10}$) based on the elemental composition (SI Table S4 and S5). The data was fit to the model with MATLAB's differential equation functions (SI Fig. S12 and S13), providing the final equation:

$$r_{CO_2} = 10^{-1.13}\exp\left(\frac{-25.3}{RT}\right)[FW][O_2]^{0.65} \quad (2)$$

The lumped model allowed insights beyond reactor capabilities (T > 450 °C) and resolution within the oxidant loading space. Uncertainty values for each parameter were calculated in MATLAB and are described in the SI.

4.4. Mineralization of CO_2 into $CaCO_3$

The mineralization studies were conducted in a second custom Parr 4561 moveable head reaction vessel. The vessel had an internal volume of 250 ml and was lined with Teflon to eliminate the negative effects of caustic solutions on the 316 stainless steel reactor body.[64] High-purity calcium hydroxide was used in these studies to maintain a caustic environment (pH > 7), necessary to allow CO_2 to dissolve into water as bicarbonate (HCO_3^-) or carbonate (CO_3^{2-}) ions which can readily react with free calcium (Ca^{2+}) to form $CaCO_3$. To test the effects of CO_2 partial pressure on mineralization, the reactor headspace experienced one of three environments: (1) pressurized to 10 atm CO_2, (2) pure CO_2

Open Access Article. Published on 23 December 2025. Downloaded on 3/14/2026 11:47:17 AM.
This article is licensed under a Creative Commons Attribution-NonCommercial 3.0 Unported Licence.

at atmospheric pressure, or (3) air (400 ppm CO_2) at atmospheric pressure. The reaction was mixed with a gas dispersion impeller for 1–120 minutes. Upon completion, the solid products were separated from the aqueous phase using vacuum filtration and were then dried in an oven at 100 °C.

4.5. $CaCO_3$ yield analysis and kinetic parameters

The resulting solid cake from mineralization experiments combined $Ca(OH)_2$ and $CaCO_3$. Using a GiegerFlex X-Ray Powder Diffractometer, a calibration curve was made to determine the weight percent of $CaCO_3$ within a sample based on the areas of characteristic peaks (SI Fig. S14). To determine the kinetic parameters of the mineralization, the $Ca(OH)_2$ was considered to be in excess due to the low solubility of $Ca(OH)_2$ in water. The initial rates of each system were determined by the method of initial rates, ($t < 20$ min), assuming the rate followed a power law equation:

$$r_{CaCO_3} = k_{CaCO_3} P^a_{CO_2} \tag{3}$$

where r_{CaCO_3} is the experimentally determined initial rates, k_{CaCO_3} is the rate constant for this system, P_{CO_2} is the partial pressure of CO_2 in the headspace, and a is the reaction order of the system with units of mol, L, atm, sec. The values of k and n were found by plotting the $\ln(r_{CaCO_3})$ *vs.* $\ln(P_{CO_2})$ which gives the equation (SI Fig. S15):

$$\ln(r_{CaCO_3}) = a\ln(P_{CO_2}) + \ln(k_{CaCO_3}) \tag{4}$$

Once k and n were solved, a family of curves could be plotted to identify the impact of CO_2 partial pressure on the conversion of $Ca(OH)_2$.

4.6. Integration of HTOM with alternative concretes

The development of HTOM was incorporated into alternative concretes in three ways: (1) the methodology laid out by Wang *et al.* in the development of ECM, (2) replacing $CaCl_2$ and Tris base with $Ca(OH)_2$ as a stoichiometric source of calcium and hydroxide ions, and (3) a control where there is no calcium or carbon introduced to the system.

For the ECM method, 0.257 g of $CaCl_2 \cdot 2H_2O$, 0.0106 g of Trizma base, 0.0813 g of Type A gelatin, and 3.13 g of 300 μm sand was mixed were added to a 0.125 m^3 cube silicone mold. Separately, a 100 ml DI water bath was heated to 35 °C, at which gelatin became soluble. Once at the temperature, 0.8 ml of the DI solution was added to the sand mixture, allowing the sand mixture to self-compress. The silicone molds were then added to a Parr vessel on top of a layer of desiccant material. The reactor was sealed, heated to 40 °C, pressurized to 10 atm of CO_2 for 2 hours, and then raised to 100 °C for 22 hours. After 24 hours, the reactor was depressurized, and the silicone molds were removed. For the $Ca(OH)_2$ system, the $CaCl_2 \cdot 2H_2O$ and Trizma base was replaced by 0.130 g of $Ca(OH)_2$, and all procedural steps were consistent with the ECM methodology.

For the control samples, the calcium and base sources were removed from the samples completely, leaving sand and gelatin remaining in the solid matrix. The pH of the aqueous media was adjusted using sodium hydroxide (NaOH) and nitric acid (HNO_3) to provide a pH ranging from 2–13. The aqueous phases were added to the mold similarly to ECM. Once added, the molds were placed directly in the oven to dry and were not exposed to CO_2.

Once dried, the uniaxial strength of each ACM block was determined by measuring its compressive strength on an Instron universal test stand, using a compression rate of 1.27 mm min^{-1}. Images of the interparticle bridging were taken on a JEOL JSM 7000F SEM. The presence of $CaCO_3$ within the samples was identified using a Netzsch 209 F1 Libra TGA with a heating rate of 5 °C min^{-1}.

4.7. Process model development

The SCWO process for converting food waste into CO_2 was modeled in ASPEN/HYSYS to estimate the overall energy flow for the system. For this model, methanol (CH_3OH) was chosen as a model compound because it has the same energy content as the food waste used (23 MJ kg^{-1}) and a similar elemental composition to food waste. The system modeled assumes 1 ton of methanol processes per day, operating continuously for 24 hours. The model uses a conversion reactor in which the operating temperature and conversion are informed by the data presented in Fig. 2d. The sum of energy demands from the pump, compressor, reactor, and steam turbine determined the net energy of the system.

4.8. Development of a lifecycle analysis

The lifecycle analysis for the waste-to-concrete process was modeled in GREET, an LCA software developed and maintained by Argonne National Laboratory (ANL). The boundary of the model includes the sourcing of food waste from landfills to the production of alternative concretes, offsetting demand from traditional concrete production (SI Fig. S16).

The model assumes that food waste is avoided from landfills, preventing landfill gas emissions. Additionally, the model is designed such that the SCWO conversion happens on-site at a waste management facility, eliminating additional transportation costs (SI Fig. S17). The energy flow of the process is dependent on the energy balance calculated by the ASPEN/HYSYS model (Fig. 4a).

The mineralization of CO_2 assumes the rapid conversion of $Ca(OH)_2$ under elevated pressures. Under batch conditions, the introduction of $Ca(OH)_2$ produced a pH that limited the strength of the model, in production, the loading of $Ca(OH)_2$ would be dosed such that the pH stayed around the peak strength.

The production of $Ca(OH)_2$ was adapted from the electrolysis process used primarily to produce sodium hydroxide. Using literature provided by ANL, the water and energy demand of the preexisting NaOH GREET process were adjusted for the conversion of calcium brines ($CaCl_2$) to form $Ca(OH)_2$, rather than sodium (NaCl) brines to form NaOH (SI Fig. S18). The emissions corresponding to sourcing of calcium brines were also adapted from GREET's existing calculations for NaCl under the assumption that the $CaCl_2$ will likely be collocated or require similar processing as NaCl (SI Fig. S19).

 © 2026 The Author(s). Published by the Royal Society of Chemistry

Open Access Article. Published on 23 December 2025. Downloaded on 3/14/2026 11:47:17 AM. This article is licensed under a Creative Commons Attribution-NonCommercial 3.0 Unported Licence.

Lastly, alternative concrete production accounts for producing and transporting sand and gelatin, the matrix and binder in these materials. Additionally, this process is awarded an associated offset for diverting production from traditional OPC (SI Fig. S20).

Author contributions

DHK designed, operated, and analyzed the SCWO, mineralization, and concrete experiments and created, analyzed, and interpreted the SCWO, ASPEN/HYSYS, and LCA models. AMC assisted in the execution of the SCWO reactions. SW and NR advised the group on alternative concrete, analysis, and manuscript writing. ART and MTT advised the study, analysis, and manuscript writing.

Conflicts of interest

The authors declare that they have no competing interests.

Abbreviation

SCWO	Supercritical Water Oxidation
CO_2	Carbon Dioxide
NET	Negative Emission Technology
MSW	Municipal Solid Waste
$CaCO_3$	Calcium Carbonate
OPC	Ordinary Portland Cement
CaO	Calcium Oxide
SiO_2	Silica/Silicon Dioxide
GWP	Global Warming Potential
ppm	Parts Per Million
BECCUS	Bioenergy Carbon Capture Utilization and Storage
HHV	Higher Heating Value
HTL	Hydrothermal Liquefaction
TOC	Total Organic Carbon
$Ca(OH)_2$	Calcium Hydroxide
DAC	Direct Air Capture
PSC	Point Source Capture
XRD	X-Ray Diffraction
HTM	Hydrothermal Mineralization
CSH	Calcium Silicate Hydrate
CaO	Calcium Oxide
$CaCl_2 \cdot 2H_2O$	Calcium Chloride Dihydrate
ECM	Enzymatic Construction
SEM	Scanning Electron Microscope
LCA	Lifecycle Assessment
MPa	Megapascals
MJ	Megajoules
kg	Kilogram
O : C	Oxygen-to-Carbon Ratio
psi	Pound per Square Inch
CR	Carbon Recovery
m_{C,CO_2}	Mass of Carbon as CO_2
$m_{C,FW}$	Mass of Carbon in Food Waste
HPLC	High-Pressure Liquid Chromatography
ODE	Ordinary Differential Equation
r_{CO_2}	Rate of Formation of CO_2 in Food Waste SCWO
Ea_{FW}	Activation Energy for Food Waste SCWO
A_{CO_2}	Pre-Exponential Factor for Food Waste SCWO
n	Reaction Order for Food Waste
m	Reaction Order for Oxygen
r_{CaCO_3}	Rate of Formation of $CaCO_3$ in Mineralization
k_{CaCO_3}	Rate Constant for $CaCO_3$ Formation
a	Reaction Order for $CaCO_3$ Mineralization
R	Ideal Gas Constant
T	Temperature
OH^-	Hydroxide Ions
HCO_3^-	Bicarbonate Ions
CO_3^{2-}	Carbonate Ions
P_{CO_2}	Partial Pressure of CO_2
HNO_3	Nitric Acid
NaOH	Sodium Hydroxide

Data availability

The collected data and developed models are available through the Teixeira Research Lab GitHub Repository, https://github.com/TeixeiraResearchLab.

Supplementary information: additional figures, detailed protocols, and raw data to support the main text. See DOI: https://doi.org/10.1039/d5su00765h.

Acknowledgements

This research was funded by the Department of Energy DE-EE0009507 along with the National Science Foundation (Grants # 1815866, and #2223664).

References

1 D. P. van Vuuren, *et al.*, Alternative pathways to the 1.5 °C target reduce the need for negative emission technologies, *Nat. Clim. Change*, 2018, **8**, 391–397, DOI: 10.1038/s41558-018-0119-8.

2 D. Cheng, *et al.*, Projecting future carbon emissions from cement production in developing countries, *Nat. Commun.*, 2023, **14**, 8213, DOI: 10.1038/s41467-023-43660-x.

3 A. Gómez-Sanabria, G. Kiesewetter, Z. Klimont, W. Schoepp and H. Haberl, Potential for future reductions of global GHG and air pollutants from circular waste management systems, *Nat. Commun.*, 2022, **13**, 106, DOI: 10.1038/s41467-021-27624-7.

4 C. Maria, J. Góis and A. Leitão, Challenges and perspectives of greenhouse gases emissions from municipal solid waste management in Angola, *Energy Rep.*, 2020, **6**, 364–369, DOI: 10.1016/j.egyr.2019.08.074.

5 S. Kaza, L. Yao, P. Bhada-Tata and F. Van Woerden *What a Waste 2.0: A Global Snapshot of Solid Waste Management to 2050*, World Bank Publications, 2018.

6 N. Tkachenko, *et al.*, Global database of cement production assets and upstream suppliers, *Sci. Data*, 2023, **10**, 696, DOI: 10.1038/s41597-023-02599-w.

7 M. Peplow, The race to upcycle CO_2 into fuels, concrete and more, *Nature*, 2022, **603**, 780–783, DOI: 10.1038/d41586-022-00807-y.

Open Access Article. Published on 23 December 2025. Downloaded on 3/14/2026 11:47:17 AM.
This article is licensed under a Creative Commons Attribution-NonCommercial 3.0 Unported Licence.

8 O. Cavalett, M. D. B. Watanabe, M. Voldsund, S. Roussanaly and F. Cherubini, Paving the way for sustainable decarbonization of the European cement industry, *Nat Sustainability*, 2024, **7**, 568–580, DOI: 10.1038/s41893-024-01320-y.
9 K. Vance, *et al.*, Direct Carbonation of Ca(OH)2 Using Liquid and Supercritical CO2: Implications for Carbon-Neutral Cementation, *Ind. Eng. Chem. Res.*, 2015, **54**, 8908–8918, DOI: 10.1021/acs.iecr.5b02356.
10 H. Ostovari, A. Sternberg and A. Bardow, Rock 'n' use of CO2: carbon footprint of carbon capture and utilization by mineralization, *Sustain. Energy Fuels*, 2020, **4**, 4482–4496, DOI: 10.1039/D0SE00190B.
11 L. McDonald, F. P. Glasser and M. S. Imbabi, A New, Carbon-Negative Precipitated Calcium Carbonate Admixture (PCC-A) for Low Carbon Portland Cements, *Materials*, 2019, **12**(4), 554.
12 C. R. Gagg, Cement and concrete as an engineering material: An historic appraisal and case study analysis, *Eng. Fail. Anal.*, 2014, **40**, 114–140, DOI: 10.1016/j.engfailanal.2014.02.004.
13 M. S. Imbabi, C. Carrigan and S. McKenna, Trends and developments in green cement and concrete technology, *Int. J. Sustain. Built Environ.*, 2012, **1**, 194–216, DOI: 10.1016/j.ijsbe.2013.05.001.
14 A. Naqi and J. G. Jang, Recent Progress in Green Cement Technology Utilizing Low-Carbon Emission Fuels and Raw Materials: A Review, *Sustainability*, 2019, **11**(2), 537.
15 G. Churkina, *et al.*, Buildings as a global carbon sink, *Nat Sustainability*, 2020, **3**, 269–276, DOI: 10.1038/s41893-019-0462-4.
16 *National Overview: Facts and Figures on Materials, Wastes and Recycling*, 2022, https://www.epa.gov/facts-and-figures-about-materials-waste-and-recycling/national-overview-facts-and-figures-materials.
17 *Understanding Global Warming Potentials*, 2023, https://www.epa.gov/ghgemissions/understanding-global-warming-potentials.
18 Y. Wang, *et al.*, Methane emissions from landfills differentially underestimated worldwide, *Nat Sustainability*, 2024, **7**, 496–507, DOI: 10.1038/s41893-024-01307-9.
19 R. N. A. Chaudhary and X. Xue Romeiko, *From Farm to Kitchen: the Environmental Impacts of U.S. Food Waste. Report No. EPA 600-R21 171*, 2021.
20 S. Budinis, S. McCulloch, P. Bains, S. Bennet, F. Briens, M. Fajardy, A. Fernandez Pales, C. Greenfield, I. Hannula, K. Kochhar, L. Lo Re, S. Moarif, R. Moore, M. Pisciotta and U. Remme, *Timur GuelDirect Air Capture: A Key Technology for Net Zero*, IEA, Paris, 2022.
21 K. Madhu, S. Pauliuk, S. Dhathri and F. Creutzig, Understanding environmental trade-offs and resource demand of direct air capture technologies through comparative life-cycle assessment, *Nat. Energy*, 2021, **6**, 1035–1044, DOI: 10.1038/s41560-021-00922-6.
22 G. Gadikota, Carbon mineralization pathways for carbon capture, storage and utilization, *Commun. Chem.*, 2021, **4**, 23, DOI: 10.1038/s42004-021-00461-x.
23 S.-Y. Pan, *et al.*, CO2 mineralization and utilization by alkaline solid wastes for potential carbon reduction, *Nat Sustainability*, 2020, **3**, 399–405, DOI: 10.1038/s41893-020-0486-9.
24 M. Stillings, Z. K. Shipton and R. J. Lunn, Mechanochemical processing of silicate rocks to trap CO2, *Nat Sustainability*, 2023, **6**, 780–788, DOI: 10.1038/s41893-023-01083-y.
25 B. M. Tackett, E. Gomez and J. G. Chen, Net reduction of CO2 *via* its thermocatalytic and electrocatalytic transformation reactions in standard and hybrid processes, *Nat. Catal.*, 2019, **2**, 381–386, DOI: 10.1038/s41929-019-0266-y.
26 G. B. David Styles, E. Ofori, C. Hennig, C. Bang, K. Koponen, G. Berndes and A. Cowie, *BECCUS Science & Policy WP7 Summary Report*, IEA Bioenergy Technology Collaboration Programme, 2025.
27 P. A. Marrone, Supercritical water oxidation—Current status of full-scale commercial activity for waste destruction, *J. Supercrit. Fluids*, 2013, **79**, 283–288, DOI: 10.1016/j.supflu.2012.12.020.
28 V. Vadillo, J. Sánchez-Oneto, J. R. Portela and E. J. Martínez de la Ossa, Problems in Supercritical Water Oxidation Process and Proposed Solutions, *Ind. Eng. Chem. Res.*, 2013, **52**, 7617–7629, DOI: 10.1021/ie400156c.
29 Y. Li, *et al.*, Supercritical water oxidation for the treatment and utilization of organic wastes: Factor effects, reaction enhancement, and novel process, *Environ. Res.*, 2024, **251**, 118571, DOI: 10.1016/j.envres.2024.118571.
30 H. O. LeClerc, *et al.*, Elucidating the role of reactive nitrogen intermediates in hetero-cyclization during hydrothermal liquefaction of food waste, *Green Chem.*, 2022, **24**, 5125–5141, DOI: 10.1039/D2GC01135B.
31 H. O. LeClerc, *et al.*, Hydroxyapatite catalyzed hydrothermal liquefaction transforms food waste from an environmental liability to renewable fuel, *iScience*, 2022, 104916, DOI: 10.1016/j.isci.2022.104916.
32 J. C. Meyer, P. A. Marrone and J. W. Tester, Acetic acid oxidation and hydrolysis in supercritical water, *AIChE J.*, 1995, **41**, 2108–2121, DOI: 10.1002/aic.690410910.
33 S. Chen, X. Qu, R. Zhang and J. Bi, Destruction of representative submarine food waste using supercritical water oxidation, *Environ. Sci. Pollut. Res.*, 2015, **22**, 4527–4533, DOI: 10.1007/s11356-014-3689-7.
34 M. Ali Khan, B. H. Hameed, M. Raza Siddiqui, Z. A. Alothman and I. H. Alsohaimi, Physicochemical properties and combustion kinetics of food waste derived hydrochars, *J. King Saud Univ. Sci.*, 2022, **34**, 101941, DOI: 10.1016/j.jksus.2022.101941.
35 M. J. Cocero, E. Alonso, M. T. Sanz and F. Fdz-Polanco, Supercritical water oxidation process under energetically self-sufficient operation, *J. Supercrit. Fluids*, 2002, **24**, 37–46, DOI: 10.1016/S0896-8446(02)00011-6.
36 T. Mizuno, M. Goto, A. Kodama and T. Hirose, Supercritical Water Oxidation of a Model Municipal Solid Waste, *Ind. Eng. Chem. Res.*, 2000, **39**, 2807–2810, DOI: 10.1021/ie0001117.
37 J. P. S. Queiroz, M. D. Bermejo, F. Mato and M. J. Cocero, Supercritical water oxidation with hydrothermal flame as internal heat source: Efficient and clean energy production

 © 2026 The Author(s). Published by the Royal Society of Chemistry

Open Access Article. Published on 23 December 2025. Downloaded on 3/14/2026 11:47:17 AM.
This article is licensed under a Creative Commons Attribution-NonCommercial 3.0 Unported Licence.

from waste, *J. Supercrit. Fluids*, 2015, **96**, 103–113, DOI: 10.1016/j.supflu.2014.09.018.

38 P. A. Marrone, S. D. Cantwell and D. W. Dalton, SCWO System Designs for Waste Treatment: Application to Chemical Weapons Destruction, *Ind. Eng. Chem. Res.*, 2005, **44**, 9030–9039, DOI: 10.1021/ie0506670.

39 J. Wilcox, P. C. Psarras and S. Liguori, Assessment of reasonable opportunities for direct air capture, *Environ. Res. Lett.*, 2017, **12**, 065001, DOI: 10.1088/1748-9326/aa6de5.

40 J. Wilcox and J. Wilcox, Introduction to carbon capture, *Carbon Capture*, 2012, pp. 1–34.

41 S. Wang, S. F. Scarlata and N. Rahbar, A self-healing enzymatic construction material, *Matter*, 2022, **5**, 957–974, DOI: 10.1016/j.matt.2021.12.020.

42 J. A. Rosewitz, S. Wang, S. F. Scarlata and N. Rahbar, An enzymatic self-healing cementitious material, *Appl. Mater. Today*, 2021, **23**, 101035, DOI: 10.1016/j.apmt.2021.101035.

43 J. Wilcox, R. Haghpanah, E. C. Rupp, J. He and K. Lee, Advancing adsorption and membrane separation processes for the gigaton carbon capture challenge, *Annu. Rev. Chem. Biomol. Eng.*, 2014, **5**, 479–505.

44 M. R. Abu Bakar, Z. K. Nagy, A. N. Saleemi and C. D. Rielly, The Impact of Direct Nucleation Control on Crystal Size Distribution in Pharmaceutical Crystallization Processes, *Cryst. Growth Des.*, 2009, **9**, 1378–1384, DOI: 10.1021/cg800595v.

45 W. Guan, Q. Qi, Z. Zhang and S. Nan, Effect of Sand Particle Size on Microstructure and Mechanical Properties of Gypsum-Cemented Similar Materials, *Materials*, 2020, **13**(3), 765, DOI: 10.3390/ma13030765.

46 S. Jain and S. K. Das, Influence of size and concentration of carbonate biomineral on biocementation and bioclogging for mitigating soil degradation, *Biogeotechnics*, 2023, **1**, 100021, DOI: 10.1016/j.bgtech.2023.100021.

47 C. M. Heveran, *et al.*, Biomineralization and Successive Regeneration of Engineered Living Building Materials, *Matter*, 2020, **2**, 481–494, DOI: 10.1016/j.matt.2019.11.016.

48 ASTM C129-22, *Specification for Nonloadbearing Concrete Masonry Units*, ASTM International, DOI: 10.1520/C0129-22.

49 ASTM C90-22, *Specification for Loadbearing Concrete Masonry Units*, ASTM International, DOI: 10.1520/C0090-01.

50 K. J. Goudie, S. J. McCreath, J. A. Parkinson, C. M. Davidson and J. J. Liggat, Investigation of the influence of pH on the properties and morphology of gelatin hydrogels, *J. Polym. Sci.*, 2023, **61**(19), 2332, DOI: 10.1002/pol.20230141.

51 A. R. Maag, *et al.*, Catalytic Hydrothermal Liquefaction of Food Waste Using CeZrOx, *Energies*, 2018, **11**(3), 564.

52 Global Industry Analysts, I. *Concrete Blocks and Bricks Manufacturing - Global Strategic Business Report*, 2024.

53 E. Korneeva, M. S. S. Mohanad, A. Babanina, E. Zaytsev and S. Poberezhskiiin *E3S Web of Conferences*, 02028, EDP Sciences, 2019.

54 H. Zhang, *Building Materials in Civil Engineering*, Woodhead Publishing, 2011, pp. 46–423.

55 H. Roedel, M. D. Lepech and D. J. Loftus in *Earth and Space 2014 Proceedings*, 2015, pp. 291–300.

56 I. Rosa, H. Roedel, M. I. Allende, M. D. Lepech and D. J. Loftus, On Designing Biopolymer-Bound Soil Composites (BSC) for Peak Compressive Strength, *J. Renewable Mater.*, 2020, **8**(8), 845–861, DOI: 10.32604/jrm.2020.09844.

57 J. Vignesh, B. Ramesh and J. R. Xavier, A review of recent trends in sustainable biopolymer-integrated concrete and its impact on mechanical performance and structural reliability, *Int. J. Biol. Macromol.*, 2025, **321**, 146408, DOI: 10.1016/j.ijbiomac.2025.146408.

58 A. Al-Atta, *et al.*, A techno-economic assessment of the potential for combining supercritical water oxidation with 'in-situ' hydrothermal synthesis of nanocatalysts using a counter current mixing reactor, *Chem. Eng. J.*, 2018, **344**, 431–440, DOI: 10.1016/j.cej.2018.03.058.

59 M. Shahabuddin, E. Italiani, A. R. Teixeira, N. Kazantzis and M. T. Timko, Roadmap for Deployment of Modularized Hydrothermal Liquefaction: Understanding the Impacts of Industry Learning, Optimal Plant Scale, and Delivery Costs on Biofuel Pricing, *ACS Sustain. Chem. Eng.*, 2023, **11**, 733–743, DOI: 10.1021/acssuschemeng.2c05982.

60 C. M. Woodall, N. McQueen, H. Pilorgé and J. Wilcox, Utilization of mineral carbonation products: current state and potential, *Greenhouse Gases: Sci. Technol.*, 2019, **9**, 1096–1113, DOI: 10.1002/ghg.1940.

61 D. Feng and A. Hicks, Environmental, human health, and CO2 payback estimation and comparison of enhanced weathering for carbon capture using wollastonite, *J. Clean. Prod.*, 2023, **414**, 137625, DOI: 10.1016/j.jclepro.2023.137625.

62 J. Skocek, M. Zajac and M. Ben Haha, Carbon Capture and Utilization by mineralization of cement pastes derived from recycled concrete, *Sci. Rep.*, 2020, **10**, 5614, DOI: 10.1038/s41598-020-62503-z.

63 S. Makjan, P. Boonsri, J. Channuie and K. Kanjana, Effects of hydrogen peroxide on 304 stainless steel in high temperature water, *J. Phys.: Conf. Ser.*, 2019, **1380**, 012087, DOI: 10.1088/1742-6596/1380/1/012087.

64 R. Davalos Monteiro, J. van de Wetering, B. Krawczyk and D. L. Engelberg, Corrosion Behaviour of Type 316L Stainless Steel in Hot Caustic Aqueous Environments, *Met. Mater. Int.*, 2020, **26**, 630–640, DOI: 10.1007/s12540-019-00403-2.